

pubs.acs.org/JPCB Article

On the Role of the Special Pair in Photosystems as a Charge Transfer Rectifier

Huseyin Aksu, Alexander Schubert, Srijana Bhandari, Atsushi Yamada, Eitan Geva, and Barry D. Dunietz*



Cite This: J. Phys. Chem. B 2020, 124, 1987-1994



ACCESS

III Metrics & More



Supporting Information

ABSTRACT: The special pair, a bacteriochlorophyll a (BChl) dimer found at the core of bacterial reaction centers, is known to play a key role in the functionality of photosystems as a precursor to the photosynthesis process. In this paper, we analyze the inherent affinity of the special pair to rectify the intrapair photo-induced charge transfer (CT). In particular, we show that the molecular environment affects the nuclear geometry, resulting in symmetry breaking between the two possible intrapair CT processes. To this end, we study the relationships of the intrapair CT and the



molecular geometry with respect to the effective dielectric constant provided by the molecular environment. We identify the special pair structural feature that breaks the symmetry between the two molecules, leading to CT rectification. Excited state energies, oscillator strengths, and electronic coupling values are obtained via time-dependent density functional theory, employing a recently developed framework based on a screened range-separated hybrid functional within a polarizable continuum model (SRSH-PCM). We analyze the rectification capability of the special pair by calculating the CT rates using a first-principles-based Fermi's golden rule approach.

■ INTRODUCTION

Significant advances in spectral and structural resolution of photosystems (PSs) contributed to our understanding of the photosynthesis process at the molecular level. ^{1–4} In particular, the charge-separation mechanism in PSs has been widely investigated using both experimental ^{5–10} and computational techniques. ¹¹ It is well established that only one of the two branches in the pseudosymmetric PSs are directly involved in the charge separation process. ^{9,12} The two branches originate at the special pair, a dimer of pigments, whose central role in the PS functionality is well established by numerous spectroscopical studies ^{11,13–16} including those of relevant dimer models. ¹⁷

However, open questions regarding the energy and charge transfer (CT) steps underlying the photosynthesis process persist including the mechanism by which the special pair is coupled to the nearby pigments of the PS. Here, we focus on structure—function relationships of the special pair in bacterial reaction centers (BRCs), which consist of two bacteriochlorophyll a (BChl) units. In particular, we study the relationship between the intrapair electron transfer and the conformational asymmetry and the dielectric environment of the pair.

We have recently studied the photoinduced CT in a series of BChl-derived dimers exploring the dependence on the intrapair distance^{18–20} and addressed the dielectric environment in BRC affecting the special-pair excitonic splitting.²¹ Computational and experimental studies indicate that an asymmetry in the special pair's electronic structure is associated with an intrapair CT process that follows its excitonic states.^{22–25} In particular, the orientation of the

functional groups is suggested to affect a symmetry broken charge density and therefore also the CT states. ^{26–28} In this study, we identify the roles of stereo asymmetry between the two BChl units and of the dielectric environment in stabilizing and discriminating between the CT processes. We use a state-of-the-art first-principles approach to calculate the special pair excited states where we follow the absorbing and the intrapair CT states as affected by the effective scalar static dielectric constant of the molecular environment. Our approach is based on a novel polarization-consistent framework that reliably addresses the dielectric environmental effects on electronic excited states by combining a screened range-separated hybrid (SRSH) functional with a polarizable continuum model (PCM). ^{29,30}

Our starting point is the X-ray study of the BRC of R. sphaeroides. Figure 1A shows the two branches, A and B, originating at the special pair where we highlight the relative orientation of the special pair units within the BRC system. Figure 1B schematically shows the stacking arrangement of the two units, where we refer to $P_{\rm A}$ and $P_{\rm B}$ by the branch the unit is closer to. Key orientational differences between the two units found in the X-ray resolved structure are also highlighted, where in $P_{\rm A}$, the functional groups noted, FG1 and FG2, are

Received: December 10, 2019 Revised: February 14, 2020 Published: February 28, 2020



Figure 1. (A) Orientational arrangement of the core pigments in BRCs of Rhodobacter sphaeroides. X-ray nuclear coordinates are taken from ref 2. (B) Distinct orientation of the two longer chain functional groups, FG1 and FG2, between the two monomers of the special pair, where in PA, the two groups are directed outward and in P_B , FG2 is pointed inward toward P_A . (C) Chemical structure of a BChl monomer. In our calculations, the residues, R_n (n = 1-3), are replaced by hydrogens.

oriented outward (away from P_B) and in P_B , only FG2 is oriented inward (towards P_A). Figure 1C identifies the BChl's chemical structure including the functional groups attached to the conjugated porphyrinic system. These functional groups, a keto ester functional group, phytyl ester with an ethylene linkage, and acetyl group are indicated in the figure as FG1, FG2, and FG3, respectively (the keto-ester is linked through both the FG1 and FG4). Below we resolve the energetic effect of these orientational differences on the intrapair CT processes. In particular, we find that FG1 and FG2 with the distinct noted orientations play a crucial role in the intrapair

Theoretical Approach and Computational Details. We investigate the effect of the molecular environment of the special pair to induce symmetry breaking and therefore rectify the photo-induced CT. The experimentally resolved structure of the special pair is reoptimized at various dielectric constants. We then calculate the electronic excited states employing a novel framework that allows to reliably address the dielectric environment at the electronic structure level $^{29-31}$ combining a SRSH functional $^{31-34}$ with a PCM. $^{35-38}$ The SRSH-PCM framework was recently used to address the condensed phase effects on the electronically excited states of BRC core pigments. 21,39

RSH functionals^{40–43} provide an excellent approach for addressing the notorious tendency of traditional density functional theory (DFT)⁴⁴⁻⁵⁰ to underestimate the fundamental orbital gap and therefore the CT state energies. 51-57 In the combined SRSH-PCM framework, ^{29,31} the environment polarization of the electron density is addressed by screening the long-range (LR) Coulombic interactions via the scalar static dielectric constant ϵ consistently through both the RSH functional parameters and the self-consistent reaction field iterations implementing the PCM. In this way, frontier orbitals retain physical significance by properly accounting for condensed phase polarization. ^{29,56} (The optical dielectric constant that affects the time-dependent DFT (TDDFT) calculations is set in all calculations to that of water, 1.78, which is reasonable for representing the embedding molecular environment of the special pair in the PS²¹). Calculated SRSH-PCM-based excited state energies were recently used successfully to study the spectra of related pigments^{21,39} and in addressing a benchmark set of CT states. Our calculated excited state energies reproduce well measured10 spectral differences due to BRC pigment pairs and excitonic splitting in the special pair.²¹

Briefly, the SRSH framework is based on expressing Coulombic interactions as

$$\frac{1}{r} = \frac{\alpha + \beta \operatorname{erf}(\gamma r)}{r} + \frac{1 - [\alpha + \beta \operatorname{erf}(\gamma r)]}{r} \tag{1}$$

where LR and short-range (SR) interactions are weighed using the functional parameters. In this more general RSH scheme, the LR interactions can be screened to represent the condensed phase dielectric environment. The SRSH functional setup follows the generalized exchange-correlation functional formulation where the energy expression is

$$E_{\text{XC}}^{\text{SRSH}} = \alpha E_{\text{F}_{\text{X}}}^{\text{SR}} + (1 - \alpha) E_{\text{DF}_{\text{X}}}^{\text{SR}} + (\alpha + \beta) E_{\text{F}_{\text{X}}}^{\text{LR}} + (1 - \alpha - \beta) E_{\text{DF}_{\text{X}}}^{\text{LR}} + E_{\text{DF}_{\text{C}}}$$
(2)

Here, the subscripts "X" and "C" denote exchange and correlation and the subscripts "F" and "DF" denote Fock exchange and a semilocal density functional of the exchange or correlation, respectively. In this SRSH exchange-correlation expression, α determines the fraction of Fock exchange in the SR and $\alpha + \beta$ determines the fraction of Fock exchange in the LR and is kept as e^{-1} . In this study, we use the ω PBE-h functional⁵⁸ as employed in earlier studies. ^{21,29,31,34,39} In this way, dielectric screening is addressed consistently by the selfconsistent reaction field responding to the dielectric constant, ϵ , with the PCM and by damping the LR exchange by the same constant in the SRSH functional. In our SRSH-PCM framework, we use the tuned range-separation parameter $\gamma =$ 0.15 bohr⁻¹ obtained by optimal tuning the special pair in the gas phase based on the $J_2(\gamma)$ scheme,⁵¹ followed by resetting the β functional parameter such that $\alpha + \beta$ equals $1/\epsilon$ with α set to 0.2.²⁹

The rates of photo-induced CT processes in the special pair are calculated at a fully quantum mechanical Fermi's goldenrule $(FGR)^{59}$ picture following our well benchmarked framework. The FGR rates are obtained by

$$k_{\text{FGR}} = \frac{|V_{\text{e}}|^2}{\hbar^2} e^{-\sum_{\alpha} S_{\alpha}(2n_{\alpha}+1)} \times \int_{-\infty}^{\infty} dt \ F_{\text{r}}^{\text{ex}}(t) \exp\left\{-\frac{i}{\hbar} \Delta E t + \sum_{\alpha} \left[(2n_{\alpha}+1) e^{-i\omega_{\alpha}t} + n_{\alpha} e^{i\omega_{\alpha}t} \right] \right) \right\}$$
(3)

In eq 3, $V_{\rm el}$ is the electronic coupling between the bright state of a high oscillator strength (OS) and the CT state of large charge separation and ΔE is the energy difference between these two states each at their optimized geometries. The electronic coupling is calculated via the fragment-charge difference (FCD) approach. 63 ω_a and S_a are the frequencies and Huang-Rhys factors 64,65 (HRFs) of the N normal modes

Table 1. Excited States of the Special Pair Obtained with RSH-PCM and SRSH-PCM Based on ω B97X-D^a

	RSH-PCM				SRSH-PCM			
ϵ	state	excitation energy (eV)	OS	charge (e)	state	excitation energy (eV)	OS	charge (e)
	S_1	1.8545	0.80	0.02	S_1	1.8709	0.72	0.02
1	S_2	1.9086	0.02	0.02	S_2	1.9225	0.02	0.02
(gas)	CT_1	2.6045	0.00	0.97	CT_1	2.3459	0.00	0.46
	CT_2	2.6493	0.00	-0.94	CT_2	2.4091	0.00	-0.65
	S_1	1.8379	1.00	0.01	CT_1	1.5247	0.12	0.89
3	S_2	1.8860	0.05	0.02	CT_2	1.5651	0.11	-0.84
(protein)	CT_1	2.6880	0.00	0.52	S_1	1.7794	0.74	-0.06
	CT_2	2.6988	0.00	-0.49	S_2	1.8058	0.05	-0.02
	S_1	1.9226	1.01	0.01	CT_1	1.3500	0.02	0.91
78	S_2	1.9685	0.05	0.02	CT_2	1.3697	0.05	-0.90
(water)	CT_1	2.7637	0.00	0.90	S_1	1.7637	0.74	-0.09
	CT_2	2.7879	0.00	-0.94	S_2	1.7945	0.02	-0.07

[&]quot;Structures are reoptimized for each dielectric constant employing PCM. For each excited state, we indicate the calculated excitation energy, OS, and the sum of the Mulliken charges of the atoms of the P_A unit.

associated with the geometrical displacement between the two minima. A diabatization of excited states into the ones of constant electronic character, that is, absorbing and CT states, is performed by means of a multi-state transformation, 66 based on diagonalization of the FCD matrix.

The structural displacement associated with a CT process is obtained as the difference between the CT-optimized geometry based on charge-constrained DFT (CDFT)-PCM and the ground state geometry assumed to represent the reactant geometry. All optimized structures are obtained by employing the dispersion-corrected ω B97X-D functional and the 6-31G** basis set within PCM with the indicated dielectric constant. In the calculation of the HRFs, we use a set of normal modes calculated at the structural minimum of each unit, where we consequently assume a negligible role of intermolecular modes in the displacement. Within the harmonic approximation, the intramolecular reorganization energy is given by $E_r = \sum_{\alpha}^{N} \hbar \omega_{\alpha} S_{\alpha}$. Lastly, n_{α} and $F_{\rm r}^{\rm ex}(t) = \exp\left[-\frac{k_{\rm B}TE_{\rm r}^{\rm ex}t^2}{\hbar^2}\right]$ are the normal modes thermal occupancies at room temperature T and outer sphere solvation, respectively, where $E_r^{\rm ex}$ is the external intermolecular reorganization energy that is found to be only 0.01 eV⁶⁹ and therefore of a negligible effect on the FGR rates. Excited states are calculated using the novel SRSH-PCM TDDFT framework³⁰ based on the ω PBE-h functional⁵⁸ with the 6-31G** basis set. For comparison, we also provide excitation energies obtained by the functional ωB97X-D with PCM representing the RSH-PCM framework.

For completeness, we compare below the FGR rates calculated using eq 3 to rates obtained at the semi-classical level of Marcus theory, which essentially 70,71 corresponds to the high-temperature and short-time limits

$$k_{\rm M} = \frac{|V_{\rm el}|^2}{\hbar^2} \sqrt{\frac{\pi}{k_{\rm B}TE_{\rm r}^{\rm tot}}} \exp\left(-\frac{(\Delta E - E_{\rm r}^{\rm tot})^2}{4k_{\rm B}TE_{\rm r}^{\rm tot}}\right) \tag{4}$$

Here, $E_{\rm r}^{\rm tot}$ = $E_{\rm r}$ + $E_{\rm r}^{\rm ex}$ includes the external intermolecular contribution to the reorganization energy, which appears to affect only negligibly the calculated rates.

The BChl molecules, as shown in Figure 1C, are simplified in our calculations by replacing the indicated residues, $R_1 - R_3$,

by hydrogens. The phytyl tails were shown to have a negligible effect on excitation energies.⁷² See also the figure for the definition of the functional groups. The electronic structure calculations are performed using the Q-Chem software package. 73

RESULTS AND DISCUSSION

Recently, the SRSH-PCM approach was shown to reproduce measured spectral peak differences associated to pairs of the core pigments in BRC, ²¹ to resolve the 2D electronic spectra of related pigments³⁹ and to reproduce well CT state energies of a well-known solvated donor-acceptor benchmark set. 30 Here, we begin by demonstrating the effectiveness of the SRSH-PCM in addressing the effects of the dielectric environment on the CT states within the pseudosymmetric special pair.

The low lying electronically excited states include two absorbing intrapair excitonic states, S₁ and S₂, and two intrapair CT states, CT₁ and CT₂, indexed by their order in excitation energy. The excitation energies, OSs, and charge transferred obtained using the RSH-PCM and SRSH-PCM levels are listed in Table 1. The lower bright excitonic state, S1, is associated with the larger OS, 10,74 while S₂ appears to be associated with a significantly smaller OS representing a semi-dark excitonic state.

As reported in earlier studies, 30 the RSH-PCM CT energies incorrectly are only marginally affected by the dielectric continuum introduced by PCM and are found to be similar to the gas phase values. CT states are expected to be strongly affected by the polarization effects of the environment. The SRSH-PCM values, on the other hand, are indeed significantly stabilized by the dielectric environment. A more complete listing of the calculated SRSH-PCM state energies at various ϵ values is provided in the Supporting Information Table S1. We proceed with the analysis based on the SRSH-PCM framework.

The frontier orbitals, highest occupied molecular orbital (HOMO), HOMO - 1, and lowest unoccupied molecular orbital (LUMO), LUMO + 1, that are involved in the four low lying excited states, are illustrated in Figure 2 with their energies at several dielectric constants. We illustrate the orbitals as calculated at $\epsilon = 2$, where their shapes remain similar at different dielectric constants. As expected these

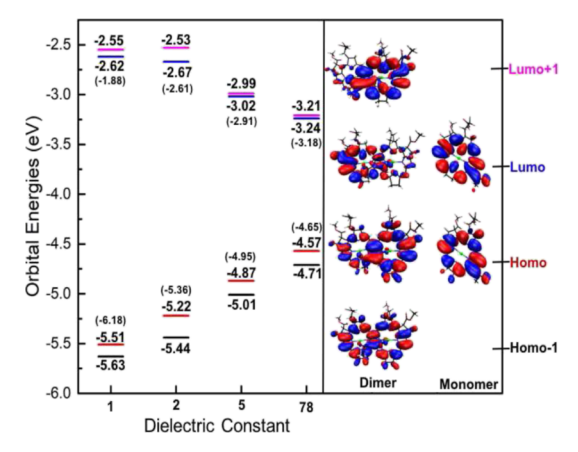


Figure 2. Special pair frontier orbital energies (eV) at different dielectric constants. BChl monomer orbital energies are noted in parentheses. The illustrated orbital densities of the special pair and a BChl-a monomer are obtained at a dielectric constant of $\epsilon=2.0$. Their shape appears similar for all ϵ values considered.

orbitals delocalize across the two monomers, reflecting the strong intermolecular coupling and the symmetric nature of the system with a HOMO–LUMO gap that decreases with the increase of the dielectric constant.

For the pair of the dark intrapair CT states, we find that in all cases the lower energy CT_1 state, $P_A{}^+P_B{}^-$, corresponds to the P_B unit serving as the acceptor, and the higher energy CT_2 state, $P_A{}^-P_B{}^+$, corresponds to the opposite CT with P_A serving as the charge acceptor. See Figure 3 for illustrations of the

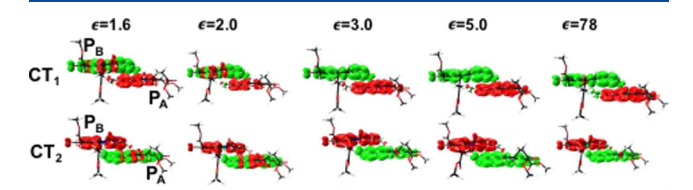


Figure 3. Detachment (red) and attachment (green) electronic densities of the CT states at different dielectric constants. The CT₁ and CT₂ correspond to $P_A^{\ \ P_B^{\ \ }}$ and $P_A^{\ \ P_B^{\ \ }}$ respectively, where CT₁ is found to be lower in energy in all calculations.

attachment—detachment electronic densities of the two CT states at various dielectric constants. Excited state properties at additional ϵ values and the major involved orbital transitions are listed in Table S1.

The excitation energies of the four low lying excited states at various dielectric constants are illustrated in Figure 4A. The calculated energies show stabilization of the CT states to below the excitonic states at dielectric constants larger than 2.0. The SRSH-PCM-calculated excited states find CT states of nearly integral electron transfer at dielectric constants, ϵ , that are smaller than 1.6 and larger than 2.0. The higher mixing of the unit densities results in smaller amounts of CT in the CT states. This larger mixing is associated with stronger coupling to the absorbing states, see the CT state attachment and detachment densities illustrated in Figure 3. At this intermediate dielectric constant region of 1.6-2.0, the CT states are partially mixed with the excitonic states and are associated with a smaller amount of CT, whereas at the other ϵ values, the CT densities are well-localized on the donoracceptor units. For example, at $\epsilon = 1.6$, the bright state shows an OS of 0.56 and a significant CT of -0.42e. The two CT states both have a significant OS of 0.2 and a CT of -0.42e and 0.62e, respectively. Importantly, we note the recently reported measured special pair excitonic splitting of 0.08 eV¹⁰ that is reproduced by the calculated 0.07 eV splitting energy with dielectric constants between 1.5 and 1.9, whereas at other dielectric constants, the calculated splitting energy is significantly smaller.2

We investigate the symmetry breaking within the special pair due to the orientational differences of the functional groups between the two units. In particular, we find that the distinct orientation of FG1 and FG2 in the two monomers as inferred from reported X-ray structures breaks the degeneracy of the CT states. 1,2 See schematic illustration of these orientational features introduced above in Figure 1B. These orientational differences are highlighted by noting the distances between the tails of FG1 and FG2. As shown in the left panel of Figure 5, this distance is relatively short with 3.9 Å in $P_{\rm A}$ and much longer with 9.0 Å in $P_{\rm B}$ (left panel).

We next relate to the role of the steric functional groups, FG1 and FG2, in affecting symmetry breaking by following the CT state energy difference. We find that the energy difference of 0.021 eV is reduced to 0.015 eV when these groups are removed and that it further decreases to 0.008 eV when the two rings are parallelly stacked, see Figure 5A–C (energies are calculated at $\epsilon=2$). Additional details are provided in the Supporting Information Table S2. We therefore find that the stereoisomerism affected by the difference in the orientations of FG1 and FG2 between the two units, which is illustrated above in Figure 1B, affects the symmetry breaking between the

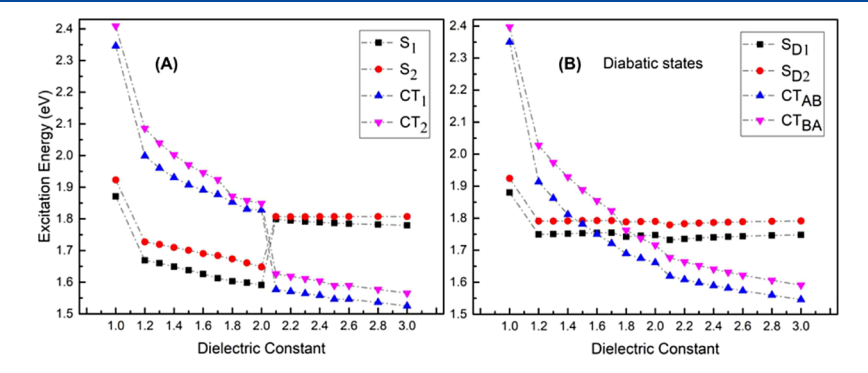


Figure 4. (A) Electronic excitation energies at different dielectric constants. States of the same character as indicated by the symbol shapes and colors are connected for clarity: excitonic bright (black square), excitonic dark (red circle), and CT states (blue and purple triangles, respectively). (B) Diabatic states presenting absorbing and CT character as obtained by multi state-FCD transformation.⁶⁶

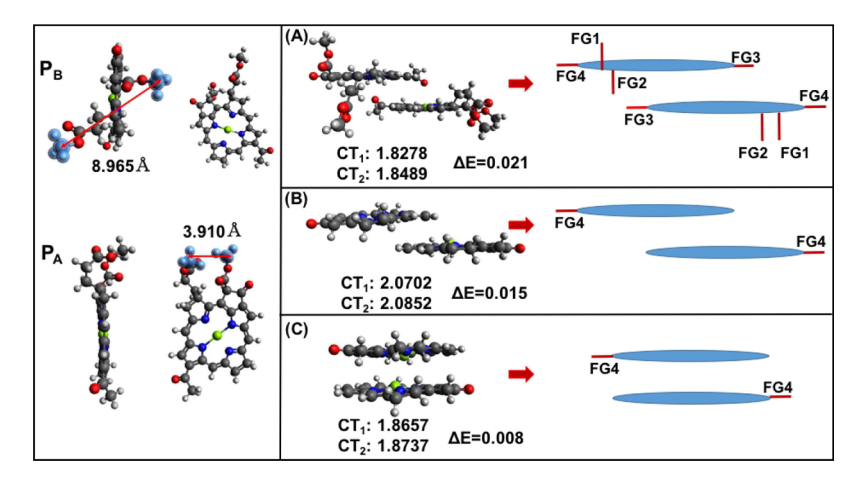


Figure 5. CT state degeneracy and symmetry breaking due to the functional groups: (left panel) the distinct orientation of the two long chain groups, FG1 and FG2, is highlighted by noting their distance of 3.9 and 9.0 Å in $P_{\rm A}$ and $P_{\rm B}$, respectively. See also addressed above in Figure 1B. (Right panel) CT state energies are calculated at $\epsilon=2.0$, where (A) all functional groups are included (B) steric functional groups are removed (only FG4 [keto] remains) (C) shifted to a fully stacked arrangement. The energy difference between the two CT states is therefore attributed mainly to the distinct orientation of FG1 and FG2.

two CT states. We turn next to the calculated CT rates and therefore the predicted CT rectification by the special pair. To this end, we use states of constant electronic character obtained using a diabatic representation.

For all dielectric constants considered, we find two excitonic states, $S_{\rm D1}$ and $S_{\rm D2}$ (where the subscript notes the relative energy), and two CT states, $CT_{\rm AB}$ and $CT_{\rm BA}$ (where the subscript notes the donor to acceptor character). The calculated diabatic excitation energies are shown above in Figure 4B. The coupling energies of the diabatic bright $S_{\rm D1}$ state to the CT states at the different dielectric constants are shown in Figure 6. The coupling energy to the $CT_{\rm AB}$ state

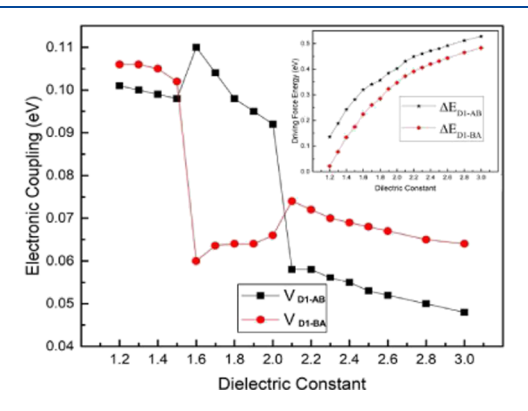


Figure 6. Coupling energies of the S_{D1} state to the CT states at various dielectric constants are presented. Inset: driving force energies, ΔE_{D1-AB} and ΔE_{D1-BA} corresponding to the differences between the excitonic state S_{D1} to the CT states. See values listed in Supporting Information Table S3.

 $(V_{\rm D1-AB})$ and the ratio with the second coupling value $(V_{\rm D1-BA})$ both maximize at the intermediate dielectric constant region where the excitonic and CT states mix. The corresponding energy biases, the energy differences between $S_{\rm D1}$ to $CT_{\rm AB}$ and $CT_{\rm BA}$ noted as $\Delta E_{\rm D1-AB}$ and $\Delta E_{\rm D1-BA}$, obtained from the diabatic states are illustrated in Figure 6 as an inset. A more complete listing of ΔE , reorganization energy, $E_{\rm r}$, activation energy, $E_{\rm a}$, and electronic coupling between $S_{\rm D1}$ and the CT states ($CT_{\rm AB}$ and $CT_{\rm BA}$), $V_{\rm el}$, and of the FGR rates is provided in Table S3. The HRF distribution associated with the highest

(at $\epsilon = 1.6$) and lowest (at $\epsilon = 78$) rates of both CT processes is provided in Supporting Information Figures S3 and S4. We also confirm that the time-dependent exponential function in the integrand of the FGR expression, eq 3, is short-lived and is therefore hardly affected by the external reorganization energy $E_{\rm r}^{\rm ex}$ that acts through the window function $F_{\rm r}^{\rm ex}(t)$, see Supporting Information Figure S5.

The rates calculated at different dielectric constants based on the diabatic states are shown in Figure 7. Importantly,

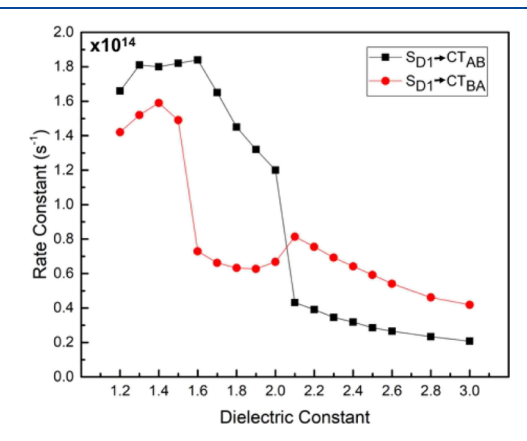


Figure 7. Calculated intrapair $S_{\rm D1}$ to $CT_{\rm AB}$ and $CT_{\rm BA}$ rate constants at the FGR level. See values listed in Supporting Information Table S3. Rates constants including at the semiclassical level calculated at a wider range of dielectric constants up to 78 are provided in Supporting Information Figures S1 and S2.

following the trend of the electronic coupling energies, at the intermediate region of the dielectric constants, 1.6–2.0, the transition rate from $S_{\rm D1}$ to $CT_{\rm AB}$ appears to maximize while the transition rate from $S_{\rm D1}$ to $CT_{\rm BA}$ appears to minimize. As a result, the rate ratio favoring the electron transfer from $P_{\rm A}$ to $P_{\rm B}$ is most pronounced at this region of dielectric constants, where it increases close to a factor of three.

Interestingly, at dielectric constants of 2.0 and higher, the rate of the opposite $P_{\rm B}$ to $P_{\rm A}$ CT process while associated with the higher energy CT state becomes relatively larger because the photo-induced dynamics follows a (slightly) inverted

regime. At the limit of the dielectric constant of water ($\varepsilon=78$), the rates attain the lowest values, see Table S2 in the Supporting Information. Note that transitions take place on such short timescales, where nonequilibrium effects in the nuclear dynamics may become significant but are not considered in the present framework. Overall, the Marcusbased ratio of the rates is in good agreement with the FGR values, even at the larger dielectric constant values that fall in the inverted regime. For completeness, we provide the rate in the larger range of dielectric constants and the semi-classical rates in the Supporting Information Figures S1–S2.

We note that the CT state associated with the transition to $P_{\rm A}^{+}P_{\rm B}^{-}$ remains the lower CT state in all considered dielectric constants. Our finding that the CT to the $P_{\rm B}$ unit is preferred as noted by the larger rate constant than that of the opposite transfer is in agreement with previous studies finding of asymmetric electronic density in the special pair. Purther studies are required to resolve the mechanism by which the special pair initiates the photosynthetic process and in particular the role of this intrapair asymmetric charge distribution, where the orientation of the nearby pigments is taken into consideration. Furthermore, also in agreement with available experimental evidence, we find that the optimal rectification of the CT within the special pair occurs at the same region of dielectric constants that offers the strongest agreement to the measured intrapair excitonic splitting. 21

We also comment on the expected time scale for the intrapair CT as derived from available experimental observations, where 2.2 ps is indicated for the charge separation producing $P^*B_A \rightarrow P^+B_A^{-10}$ The intermolecular distance within the special pair units is (plane to plane distance) ≈ 3.5 Å, whereas the distance to adjacent pigment B_A is significantly larger, with the distance of the Mg of P_B to Mg of B_A of ≈ 13 Å. We therefore assume that the intrapair CT is not the rate-determining step and therefore must occur at time scales that are faster than 2.2 ps. Indeed, internal conversion within the special pair and the calculated CT rates in this work are both found to occur at a faster range of 2-100 fs. 10,74

CONCLUSIONS

We study the structure—function relationships of the special pair that affect the intrapair CT processes. The molecular environment of the special pair stabilizes the CT states and affects the symmetry breaking through the distinct orientations of the functional groups resulting with charge rectification functionality by the special pair. We use state-of-the-art DFT that combines SRSH with PCM to calculate the special pair excited states and their coupling at varied dielectric constants to obtain energy parameters that affect the CT rates. The SRSH-PCM framework achieves polarization-consistent treatment of the electrostatic environment.

In particular, the orientational features that break the stereosymmetry within the special pair in BRC and lift the degeneracy of the CT states are identified. The orientation of the side groups as indicated in their X-ray resolved structures is addressed in the calculation of the excited states. We find that the different orientations of the long chain functional groups phytyl ester (indicated above as FG1 and FG2) affect symmetry breaking between the two intrapair CT states. The intrapair electron transfer rates are then calculated using a FGR level of theory at various dielectric constants, where we find the photoinduced generation of $P_{\rm A}{}^{+}P_{\rm B}{}^{-}$ rate to be both the largest and with the highest favorable ratio over the opposite CT

process at the dielectric constants of 1.6–1.8, that are within the range of constants that reproduce the measured excitonic splitting of the special pair states. ¹⁰ In this way, we provide a molecular level understanding on the way that the special pair structure initiates the charge separation process within the BRC. We are following up by calculating the subsequent transfer and transport steps that couple the special pair to the branches in the photosynthesis process.

ASSOCIATED CONTENT

Supporting Information

The Supporting Information is available free of charge at https://pubs.acs.org/doi/10.1021/acs.jpcb.9b11431.

Table of numerical values associated with the electronic states represented in the figures, the CT rate constants up to a dielectric constant of 78, and the atomic coordinates of the special pair and of the monomers (PDF)

AUTHOR INFORMATION

Corresponding Author

Barry D. Dunietz — Department of Chemistry and Biochemistry, Kent State University, Kent, Ohio 44242, United States;
o orcid.org/0000-0002-6982-8995; Phone: +1 330 6722032; Email: bdunietz@kent.edu; Fax: +1 330 6723816

Authors

Huseyin Aksu — Department of Chemistry and Biochemistry, Kent State University, Kent, Ohio 44242, United States; occid.org/0000-0001-9463-3236

Alexander Schubert — Department of Chemistry and Biochemistry, Kent State University, Kent, Ohio 44242, United States; Department of Chemistry, University of Michigan, Ann Arbor, Michigan 48109, United States; orcid.org/0000-0002-8560-6436

Srijana Bhandari — Department of Chemistry and Biochemistry, Kent State University, Kent, Ohio 44242, United States

Atsushi Yamada — Center for Computational Sciences,
University of Tsukuba, Tsukuba, Ibaraki 305-8577, Japan

Eitan Geva — Department of Chemistry, University of Michigan,
Ann Arbor, Michigan 48109, United States; orcid.org/
0000-0002-7935-4586

Complete contact information is available at: https://pubs.acs.org/10.1021/acs.jpcb.9b11431

Notes

The authors declare no competing financial interest.

ACKNOWLEDGMENTS

B.D.D. and E.G. are grateful for support by DOE Basic Energy Sciences through the Chemical Sciences Geosciences and Biosciences Division, through grant no. DE-SC0016501. A.S. is grateful for support from an ICAM fellowship, awarded by the Kent State University and University of Michigan ICAM branches. We are thankful to the Ohio supercomputer⁷⁷ and the Kent State University College of Arts and Sciences for computing facilities and making the resources available to complete the reported research.

REFERENCES

(1) Ermler, U.; Fritzsch, G.; Buchanan, S. K.; Michel, H. Structure of the Photosynthetic Reaction Centre From Rhodobacter Sphaeroides

- at 2.65 Å Resolution: Cofactors and Protein-Cofactor Interactions. Structure 1994, 2, 925–936.
- (2) Koepke, J.; Krammer, E.-M.; Klingen, A. R.; Sebban, P.; Ullmann, G. M.; Fritzsch, G. pH Modulates the Quinone Position in the Photosynthetic Reaction Center from Rhodobacter sphaeroides in the Neutral and Charge Separated States. *J. Mol. Biol.* **2007**, *371*, 396–409.
- (3) Vacha, F.; Joseph, D. M.; Durrant, J. R.; Telfer, A.; Klug, D. R.; Barber, J. Photochemistry and Spectroscopy of a Five-Chlorophyll Reaction Center of Photosystem II Isolated by Using a Cu Affinity Column. *Proc. Natl. Acad. Sci. U.S.A.* **1995**, 92, 2929–2933.
- (4) Brixner, T.; Hildner, R.; Köhler, J.; Lambert, C.; Würthner, F. Exciton Transport in Molecular Aggregates From Natural Antennas to Synthetic Chromophore Systems. *Adv. Energy Mater.* **2017**, *7*, 1700236.
- (5) Van Brederode, M. E.; Jones, M. R.; Van Mourik, F.; Van Stokkum, I. H. M.; Van Grondelle, R. A New Pathway for Transmembrane Electron Transfer in Photosynthetic Reaction Centers of Rhodobacter sphaeroides Not Involving the Excited Special Pair. *Biochemistry* 1997, 36, 6855–6861.
- (6) Vos, M. H.; Rappaport, F.; Lambry, J.-C.; Breton, J.; Martin, J.-L. Visualization of Coherent Nuclear Motion in a Membrane Protein by Femtosecond Spectroscopy. *Nature* **1993**, *363*, 320–325.
- (7) Novoderezhkin, V. I.; Yakovlev, A. G.; van Grondelle, R.; Shuvalov, V. A. Coherent Nuclear and Electronic Dynamics in Primary Charge Separation in Photosynthetic Reaction Centers: A Redfield Approach. *J. Phys. Chem. B* **2004**, *108*, 7445–7457.
- (8) Romero, E.; Novoderezhkin, V. I.; van Grondelle, R. Quantum Design of Photosynthesis for Bio-Inspired Solar-Energy Conversion. *Nature* **2017**, *543*, 355.
- (9) Steffen, M. A.; Lao, K.; Boxer, S. G. Dielectric Asymmetry in the Photosynthetic Reaction Center. *Science* **1994**, 264, 810–816.
- (10) Niedringhaus, A.; Policht, V. R.; Sechrist, R.; Konar, A.; Laible, P. D.; Bocian, D. F.; Holten, D.; Kirmaier, C.; Ogilvie, J. P. Primary Processes in the Bacterial Reaction Center Probed by Two-Dimensional Electronic Spectroscopy. *Proc. Natl. Acad. Sci. U.S.A.* **2018**, *115*, 3563–3568.
- (11) Jordanides, X. J.; Scholes, G. D.; Fleming, G. R. The Mechanism of Energy Transfer in the Bacterial Photosynthetic Reaction Center. J. Phys. Chem. B 2001, 105, 1652–1669.
- (12) Saggu, M.; Fried, S. D.; Boxer, S. G. Local and Global Electric Field Asymmetry in Photosynthetic Reaction Centers. *J. Phys. Chem. B* **2019**, *123*, 1527–1536.
- (13) Hasegawa, J.; Ohkawa, K.; Nakatsuji, H. Excited States of the Photosynthetic Reaction Center of Rhodopseudomonas viridis: SACCI Study. *J. Phys. Chem. B* **1998**, *102*, 10410–10419.
- (14) Warshel, A.; Parson, W. W. Spectroscopic Properties of Photosynthetic Reaction Centers. 1. Theory. *J. Am. Chem. Soc.* **1987**, 109, 6143–6152.
- (15) Parson, W. W.; Warshel, A. Spectroscopic Properties of Photosynthetic Reaction Centers. 2. Application of the Theory to Rhodopseudomonas Viridis. *J. Am. Chem. Soc.* **1987**, *109*, 6152–6163.
- (16) Zinth, W.; Wachtveitl, J. The First Picoseconds in Bacterial Photosynthesis—Ultrafast Electron Transfer for the Efficient Conversion of Light Energy. *ChemPhysChem* **2005**, *6*, 871–880.
- (17) Song, J.; Gao, F.; Liang, W. How Does the Nonlocal HF Exchange Influence the Electron Excitation of Bacteriochlorophyll and Its Assembly. *Comput. Theor. Chem.* **2011**, *965*, 53–59.
- (18) Manna, A. K.; Dunietz, B. D. Communication: Charge-transfer Rate Constants in Zinc-Porphyrin-Porphyrin-derived dyads: A Fermi Golden Rule First-Principles-Based Study. *J. Chem. Phys.* **2014**, *141*, 121102.
- (19) Manna, A. K.; Balamurugan, D.; Cheung, M. S.; Dunietz, B. D. Unraveling the Mechanism of Photoinduced Charge Transfer in Carotenoid Porphyrin C60 Molecular Triad. *J. Phys. Chem. Lett.* **2015**, *6*, 1231–1237.
- (20) McCleese, C.; Yu, Z.; Esemoto, N. N.; Kolodziej, C.; Maiti, B.; Bhandari, S.; Dunietz, B. D.; Burda, C.; Ptaszek, M. Excitonic Interactions in Bacteriochlorin Homo-Dyads Enable Charge Transfer:

- A New Approach to the Artificial Photosynthetic Special Pair. *J. Phys. Chem. B* **2018**, *122*, 4131–4140.
- (21) Aksu, H.; Schubert, A.; Geva, E.; Dunietz, B. D. Explaining Spectral Asymmetries and Excitonic Characters of the Core Pigment Pairs in the Bacterial Reaction Center Using Screened Range-Separated Hybrid Functionals. *J. Phys. Chem. B* **2019**, *123*, 8970–8975.
- (22) Wawrzyniak, P. K.; Beerepoot, M. T. P.; de Groot, H. J. M.; Buda, F. Acetyl Group Orientation Modulates the Electronic Ground-State Asymmetry of the Special Pair in Purple Bacterial Reaction Centers. *Phys. Chem. Chem. Phys.* **2011**, *13*, 10270–10279.
- (23) Moore, L. J.; Zhou, H.; Boxer, S. G. Excited-State Electronic Asymmetry of the Special Pair in Photosynthetic Reaction Center Mutants: Absorption and Stark Spectroscopy. *Biochemistry* **1999**, *38*, 11949–11960.
- (24) Lockhart, D. J.; Boxer, S. G. Stark Effect Spectroscopy of Rhodobacter Sphaeroides and Rhodopseudomonas Viridis Reaction Centers. *Proc. Natl. Acad. Sci. U.S.A.* **1988**, 85, 107–111.
- (25) Lendzian, F.; Huber, M.; Isaacson, R. A.; Endeward, B.; Plato, M.; Bönigk, B.; Möbius, K.; Lubitz, W.; Feher, G. The Electronic Structure of the Primary Donor Cation Radical in Rhodobacter Sphaeroides R-26: ENDOR and TRIPLE Resonance Studies in Single Crystals of Reaction Centers. *Biochim. Biophys. Acta* 1993, 1183, 139–160.
- (26) Yamasaki, H.; Nakamura, H.; Takano, Y. Theoretical Analysis of the Electronic Asymmetry of the Special Pair in the Photosynthetic Reaction Center: Effect of Structural Asymmetry and Protein Environment. *Chem. Phys. Lett.* **2007**, *447*, 324–329.
- (27) Yamasaki, H.; Takano, Y.; Nakamura, H. Theoretical Investigation of the Electronic Asymmetry of the Special Pair Cation Radical in the Photosynthetic Type-II Reaction Center. *J. Phys. Chem. B* **2008**, *112*, 13923–13933.
- (28) Sai Sankar Gupta, K. B.; Alia, A.; de Groot, H. J. M.; Matysik, J. Symmetry Break of Special Pair: Photochemically Induced Dynamic Nuclear Polarization NMR Confirms Control by Nonaromatic Substituents. *J. Am. Chem. Soc.* **2013**, *135*, 10382–10387.
- (29) Bhandari, S.; Cheung, M. S.; Geva, E.; Kronik, L.; Dunietz, B. D. Fundamental Gaps of Condensed-Phase Organic Semiconductors From Single-Molecule Polarization-Consistent Optimally Tuned Screened Range-Separated Hybrid Functionals. *J. Chem. Theory Comput.* 2018, 14, 6287–6294.
- (30) Bhandari, S.; Dunietz, B. D. Quantitative Accuracy in Calculating Charge Transfer State Energies in Solvated Molecular Dimers Using Screened Range Separated Hybrid Functional Within a Polarized Continuum Model. *J. Chem. Theory Comput.* **2019**, *15*, 4305.
- (31) Joo, B.; Han, H.; Kim, E.-G. Self-Sufficiency through Screened Exchange. *J. Chem. Theory Comput.* **2018**, *14*, 2823–2828.
- (32) Kronik, L.; Kümmel, S. Dielectric Screening Meets Optimally-Tuned Density Functionals. *Adv. Mater.* **2018**, *30*, 1706560.
- (33) Refaely-Abramson, S.; Jain, M.; Sharifzadeh, S.; Neaton, J. B.; Kronik, L. Solid-State Optical Absorption From Optimally Tuned Time-Dependent Range-Separated Hybrid Density Functional Theory. *Physical Review B: Condensed Matter and Materials Physics* 2015, 92, 081204–081209.
- (34) Zheng, Z.; Egger, D. A.; Brédas, J.-L.; Kronik, L.; Coropceanu, V. Effect of Solid-State Polarization on Charge-Transfer Excitations and Transport Levels at Organic Interfaces From a Screened Range-Separated Hybrid Functional. *J. Phys. Chem. Lett.* **2017**, *8*, 3277–3283.
- (35) Tannor, D.; Marten, B.; Murphy, R.; Ringnalda, M.; Friesner, R. A.; Nicholls, A.; Goddard, W. A., III; Honig, B. Accurate Calculation of Charge Distributions and Solvation Energies with Ab Initio Quantum Mechanics and Dielectric Continuum Theory. *J. Am. Chem. Soc.* **1994**, *116*, 11875.
- (36) Mennucci, B.; Tomasi, J. Continuum Solvation Models: A new Approach to the Problem of Solute's Charge Distribution and Cavity Boundaries. *J. Chem. Phys.* **1997**, *106*, 5151–5158.

- (37) Tomasi, J.; Mennucci, B.; Cammi, R. Quantum Mechanical Continuum Solvation Models. *Chem. Rev.* **2005**, *105*, 2999–3094.
- (38) Takano, Y.; Houk, K. N. Benchmarking the Conductor-Like Polarizable Continuum Model (CPCM) for Aqueous Solvation Free Energies of Neutral and Ionic Organic Molecules. *J. Chem. Theory Comput.* **2005**, *1*, 70–77.
- (39) Song, Y.; Schubert, A.; Maret, E.; Burdick, R. K.; Dunietz, B. D.; Geva, E.; Ogilvie, J. P. Vibronic Structure of Photosynthetic Pigments Probed by Polarized Two-Dimensional Electronic Spectroscopy and Ab Initio Calculations. *Chem. Sci.* **2019**, *10*, 8143.
- (40) Tawada, Y.; Tsuneda, T.; Yanagisawa, S.; Yanai, T.; Hirao, K. A Long-Range-Corrected Time-Dependent Density Functional Theory. *J. Chem. Phys.* **2004**, *120*, 8425–8433.
- (41) Baer, R.; Neuhauser, D. Density Functional Theory with Correct Long-Range Asymptotic Behavior. *Phys. Rev. Lett.* **2005**, 94, 043002.
- (42) Yanai, T.; Tew, D. P.; Handy, N. C. A New Hybrid Exchange-Correlation Functional Using Coulomb-Attenuating Method (CAM-B3LYP). *Chem. Phys. Lett.* **2004**, 393, 51–57.
- (43) Kümmel, S.; Kronik, L. Orbital-Dependent Density Functionals: Theory and Applications. *Rev. Mod. Phys.* **2008**, *80*, 3–60.
- (44) Perdew, J. P.; Burke, K.; Ernzerhof, M. Generalized Gradient Approximation Made Simple. *Phys. Rev. Lett.* **1996**, *77*, 3865.
- (45) Sham, L. J.; Schlüter, M. Density Functional Theory of the Gap. *Phys. Rev. Lett.* **1983**, *51*, 1888–1891.
- (46) Tozer, D. J. Relationship Between Long-Range Charge-Transfer Excitation Energy Error and Integer Discontinuity in Kohn-Sham Theory. *J. Chem. Phys.* **2003**, *119*, 12697–12699.
- (47) Teale, A. M.; De Proft, F.; Tozer, D. J. Orbital Energies and Negative Electron Affinities From Density Functional Theory: Insight From the Integer Discontinuity. *J. Chem. Phys.* **2008**, *129*, 044110.
- (48) Seidl, A.; Görling, A.; Vogl, P.; Majewski, J. A.; Levy, M. Generalized Kohn-Sham Schemes and the Band-Gap Problem. *Physical Review B: Condensed Matter and Materials Physics* **1996**, 53, 3764–3774.
- (49) Kronik, L.; Stein, T.; Refaely-Abramson, S.; Baer, R. Excitation Gaps of Finite-Sized Systems from Optimally Tuned Range-Separated Hybrid Functionals. *J. Chem. Theory Comput.* **2012**, *8*, 1515–1531.
- (50) Chai, J.-D.; Chen, P.-T. Restoration of the Derivative Discontinuity in Kohn-Sham Density Functional Theory: An Efficient Scheme for Energy Gap Correction. *Phys. Rev. Lett.* **2013**, *110*, 033002.
- (51) Stein, T.; Kronik, L.; Baer, R. Prediction of Charge-Transfer Excitations in Coumarin-Based Dyes Using a Range-Separated Functional Tuned From First Principles. *J. Chem. Phys.* **2009**, *131*, 244119.
- (52) Stein, T.; Eisenberg, H.; Kronik, L.; Baer, R. Fundamental Gaps in Finite Systems from Eigenvalues of a Generalized Kohn-Sham Method. *Phys. Rev. Lett.* **2010**, *105*, 266802.
- (53) Phillips, H.; Geva, E.; Dunietz, B. D. Calculating Off-Site Excitations in Symmetric Donor-Acceptor Systems Via Time-Dependent Density Functional Theory With Range-Separated Density Functionals. *J. Chem. Theory Comput.* **2012**, *8*, 2661–2668.
- (54) Zheng, S.; Phillips, H.; Geva, E.; Dunietz, B. D. Ab-initio Study of the Emissive Charge-Transfer States of Solvated Chromophore-Functionalized Silsesquioxanes. *J. Am. Chem. Soc.* **2012**, *134*, 6944–6947.
- (55) Zheng, S.; Geva, E.; Dunietz, B. D. Solvated Charge Transfer States of Functionalized Anthracene and Tetracyanoethylene Dimers: A Computational Study based on a Range Separated Hybrid Functional and Charge Constrained Self-consistent Field with Switching Gaussian Polarized Continuum Models. J. Chem. Theory Comput. 2013, 9, 1125–1131.
- (56) Phillips, H.; Zheng, Z.; Geva, E.; Dunietz, B. D. Orbital Gap Predictions for Rational Design of Organic Photovoltaic Materials. *Org. Electron.* **2014**, *15*, 1509–1520.
- (57) Manna, A. K.; Lee, M. H.; McMahon, K. L.; Dunietz, B. D. Calculating High Energy Charge Transfer States Using Optimally

- Tuned Range-Separated Hybrid Functionals. J. Chem. Theory Comput. **2015**, 11, 1110–1117.
- (58) Rohrdanz, M. A.; Martins, K. M.; Herbert, J. M. A Long-Range-Corrected Density Functional That Performs Well for Both Ground-State Properties and Time-Dependent Density Functional Theory Excitation Energies, Including Charge-Transfer Excited States. *J. Chem. Phys.* **2009**, *130*, 054112–054119.
- (59) Barbara, P. F.; Meyer, T. J.; Ratner, M. A. Contemporary Issues in Electron Transfer Research. *J. Phys. Chem.* **1996**, *100*, 13148–13168.
- (60) Lee, M. H.; Dunietz, B. D.; Geva, E. Donor-to-Donor vs Donor-to-Acceptor Interfacial Charge Transfer States in the Phthalocyanine—Fullerene Organic Photovoltaic System. *J. Phys. Chem. Lett.* **2014**, *5*, 3810–3816.
- (61) Lee, M. H.; Geva, E.; Dunietz, B. D. Calculation from First-Principles of Golden Rule Rate Constants for Photoinduced Subphthalocyanine/Fullerene Interfacial Charge Transfer and Recombination in Organic Photovoltaic Cells. *J. Phys. Chem. C* **2014**, *118*, 9780–9789.
- (62) Lee, M. H.; Geva, E.; Dunietz, B. D. The Effect of Interfacial Geometry on Charge-Transfer States in the Phthalocyanine/Fullerene Organic Photovoltaic System. *J. Phys. Chem. A* **2016**, *120*, 2970–2975.
- (63) Voityuk, A. A.; Rösch, N. Fragment Charge Difference Method for Estimating Donor—Acceptor Electronic Coupling: Application to DNA π -Stacks. *J. Chem. Phys.* **2002**, *117*, 5607—5616.
- (64) Nitzan, A. Chemical Dynamics in Condensed Phases: Relaxation, Transfer and Reactions in Condensed Molecular Systems; Oxford university press, 2006.
- (65) Huang, K.; Rhys, A. Theory of Light Absorption and Non-Radiative Transitions in F-Centres. *Proc. R. Soc. A* **1950**, 204, 406–423.
- (66) Yang, C.-H.; Hsu, C.-P. A Multi-State Fragment Charge Difference Approach for Diabatic States in Electron Transfer: Extension and Automation. *J. Chem. Phys.* **2013**, *139*, 154104.
- (67) Wu, Q.; Van Voorhis, T. Direct Optimization Method to Study Constrained Systems Within Density-Functional Theory. *Phys. Rev. A* **2005**, 72, 024502–024505.
- (68) Chai, J.-D.; Head-Gordon, M. Long-Range Corrected Hybrid Density Functionals With Damped Atom-Atom Dispersion Corrections. *Phys. Chem. Chem. Phys.* **2008**, *10*, 6615.
- (69) Kee, H. L.; Diers, J. R.; Ptaszek, M.; Muthiah, C.; Fan, D.; Lindsey, J. S.; Bocian, D. F.; Holten, D. Chlorin—Bacteriochlorin Energy-transfer Dyads as Prototypes for Near-infrared Molecular Imaging Probes: Controlling Charge-Transfer and Fluorescence Properties in Polar Media. *Photochem. Photobiol.* **2009**, *85*, 909—920.
- (70) Marcus, R. A. On the Theory of Oxidation-Reduction Reactions Involving Electron Transfer. I. *J. Chem. Phys.* **1956**, 24, 966–978.
- (71) Marcus, R. A. Electron Transfer Reactions in Chemistry. Theory and Experiment. *Rev. Mod. Phys.* **1993**, *65*, 599–610.
- (72) Kenny, E. P.; Kassal, I. Benchmarking Calculations of Excitonic Couplings between Bacteriochlorophylls. *J. Phys. Chem. B* **2016**, *120*, 25–32.
- (73) Shao, Y.; et al. Advances in Methods and Algorithms in a Modern Quantum Chemistry Program Package. *Phys. Chem. Chem. Phys.* **2006**, *8*, 3172–3191.
- (74) Khmelnitskiy, A.; Reinot, T.; Jankowiak, R. Mixed Upper Exciton State of the Special Pair in Bacterial Reaction Centers. *J. Phys. Chem. B* **2019**, *123*, 852–859.
- (75) Sun, X.; Geva, E. Nonequilibrium Fermi's Golden Rule Charge Transfer Rates via the Linearized Semiclassical Method. *J. Chem. Theory Comput.* **2016**, *12*, 2926–2941.
- (76) Kananenka, A. A.; Sun, X.; Schubert, A.; Dunietz, B. D.; Geva, E. A Comparative Study of Different Methods for Calculating Electronic Transition Rates. *J. Chem. Phys.* **2018**, *148*, 102304.
- (77) Ohio Supercomputer Center. http://osc.edu/ark:/19495/f5s1ph73, 1987.